International Journal of Thermophysics, Vol. 19, No. 4, 1998

Analysis of the Photoacoustic Detector Signal for Thermal Diffusivities of Gases[1]

J. Soldner[2,3] and K. Stephan[2]

A resonant and a nonresonant photoacoustic detector were used to determine thermal diffusivities of gases. With a nonresonant detector thermal diffusivities can be determined in a wide range between 10^{-3} and $10^{-7}\,\mathrm{m^2 \cdot s^{-1}}$, whereas experiments with the resonant detector deliver thermal diffusivities in a range that is about a factor of 100 smaller. As refrigerants—HFCs, HCFCs, and hydrocarbons—are absorbents in the infrared at a wavelength of 3.39 μm, their thermal diffusivity can be determined without the addition of a trace gas, particularly at pressures below 0.01 MPa. At pressures above 0.1 MPa, the addition of ammonia as a trace gas is recommended. The absorption wavelength is then 1.531 μm. A simulation model for the nonresonant photoacoustic detector is presented for the design of a detector and for an extended error analysis.

KEY WORDS: *photoacoustic detector; thermal conductivity; thermal diffusivity.*

1. INTRODUCTION

Transport properties such as thermal conductivity and viscosity are essential quantities for heat exchanger design, and heat-transfer coefficients for these apparatus are usually determined from correlations containing these properties.

This paper focuses on measurements of the thermal conductivity of gases at moderate pressures of 0.01 to 1.0 MPa. As is well known, the temperature-dependent thermal conductivity λ_0 of the dilute gas is of prime importance for the presentation of thermal conductivities with the aid of the residual concept [1, 2].

---

[1] Paper presented at the Thirteenth Symposium on Thermophysical Properties, June 22–27, 1997, Boulder, Colorado, U.S.A.

[2] Institut für Technische Thermodynamik und Thermische Verfahrenstechnik, Universität Stuttgart, Pfaffenwaldring 9, 70569 Stuttgart, Germany.

[3] To whom correspondence should be addressed.

0195-928X/98/0700-1099$15.00/0 © 1998 Plenum Publishing Corporation

There exists a variety of methods to measure thermal conductivities. The most common technique is the transient hot wire method [3, 4]. Results with this method, however, become inaccurate at pressures below 0.01 MPa. Other well-established methods, such as steady-state measurements with a concentric-cylinder apparatus [5], are also not applicable in the range of pressures below 0.2 MPa. In contrast, the dynamic light scattering method [6] is appropriate for thermal diffusivity measurements at high pressures, where densities are above $100 \, \mathrm{kg \cdot m^{-3}}$. An appropriate method to measure thermal diffusivities at moderate pressures is the photoacoustic technique. As shown in experiments with argon as a reference fluid, the uncertainty is below ±1 % [7]. The measured thermal diffusivity $a = \lambda/(\rho c_v)$ can be converted into the thermal conductivity with the aid of an equation of state for density ρ and isochoric heat capacity c_v.

The photoacoustic method is based on the conversion of radiation energy into an acoustic signal. In the experiments, a periodically modulated laser penetrates the sample chamber—a cylindrical cell charged with the test fluid. A small part of the radiation energy is absorbed by an absorbent added to the test gas. This absorbent is added as a trace gas in small amounts of the order of ppm, so that the thermophysical properties of the test gas are not affected. The trace gas should be a strong absorbent at the emission wavelength of the laser, so that the energy transfer between the trace gas and the test gas inside the cell induces a small rise in temperature of some millikelvins, and a pressure rise of about 1 Pa. As the laser beam is modulated periodically, and the wall temperature of the sample cell is held constant, the temperature and pressure will alternate as well. Thus, an acoustic signal, as shown in Fig. 1, is generated. It can be detected by a sensitive microphone, and the thermal diffusivity of the sample gas can be determined from the time-dependent pressure rise.

Figure 2 shows a schematic experimental setup. A detailed description of the electronic instrumentation is given elsewhere [8]. The sample chamber consists of a stainless-steel tube of 1.5 mm inner diameter and 103 mm length. It is shrunk into a copper cylinder, so that a good thermal contact is attained. The copper cylinder itself is part of a thermostat which keeps the wall of the sample chamber constant within ±1 mK. The microphone can be mounted either next to the sample chamber or, as shown in Fig. 2, outside the insulation. In the first case a high-temperature microphone is needed. It is advantageous that the photoacoustic detector is nonresonant. When the microphone is placed outside the insulation, the sample chamber, the coupling tube, and the microphone act as an acoustic resonator and exhibit damped harmonic oscillations.

Both the nonresonant and the resonant photoacoustic detectors are analyzed in the next sections. The advantages and disadvantages of each

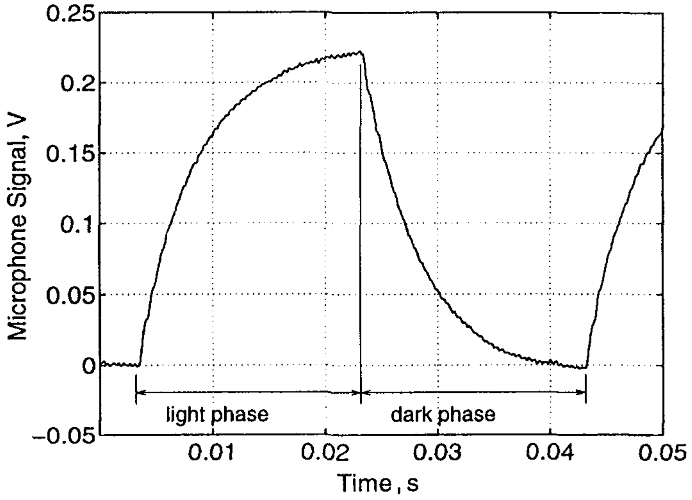

Fig. 1. The photoacoustic signal.

design, as well as their measuring ranges, are discussed. As will be shown, with refrigerants the pressure range can be extended when measurements are carried out at different wavelengths.

2. THE NONRESONANT PHOTOACOUSTIC DETECTOR

The temperature rise in a nonresonant photoacoustic detector is obtained from the equation of heat diffusion in an infinite cylinder,

$$\rho c_v \frac{\partial T}{\partial t} = \lambda \frac{\partial^2 T}{\partial r^2} + \frac{\lambda}{r}\frac{\partial T}{\partial r} + \mathscr{A}(r, z) \tag{1}$$

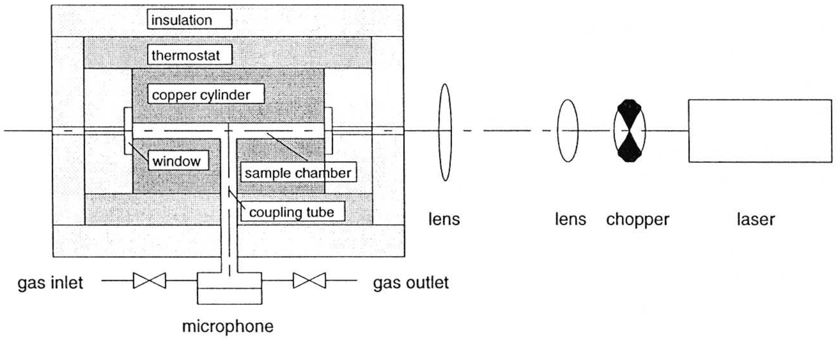

Fig. 2. The experimental setup.

with the temperature T, time t, thermal conductivity λ, the radial coordinate in the sample chamber r, and the axial coordinate z. The heat generation $\mathscr{A}$ depends on the intensity $I(r, z)$ and is given for an absorptivity below $\alpha = 0.3\ m^{-1}$ by a linear relationship,

$$\mathscr{A}(r, z) = \alpha I(r, z)$$

The intensity $I(r, z)$ of an ideal Gaussian laser beam is given by

$$I(r, z) = \frac{W}{\pi\omega(z)^2} \exp\left(-\frac{r^2}{\omega(z)^2}\right) \tag{3}$$

where W denotes the radiative power of the laser and $\omega(z)$ is defined as the radius where the beam intensity reaches $1/e$ of its peak value. The coordinate z has its origin in the beam focus. As shown by the experiments of Soldner and Stephan [8], the axial profile of the beam radius $\omega(z)$ can be approximated by

$$\omega(z) = \omega_0(1 + C^*z^2)^{1/2} \tag{4}$$

wherein the constants ω_0 and C^* are determined from measurements of the intensity distribution of the beam at various locations inside the sample chamber with the aid of a beam scanner. The boundary conditions are constant wall temperature $T(t, r = R, z) = T_w$ and rotational symmetry $(\partial T/\partial r)_{t, r=0} = 0$.

Figure 1 shows the pressure generated by means of a periodically modulated laser beam. It becomes obvious that the pressure toward the end of a light phase has not reached its limit, where all radiation energy absorbed by the fluid is transferred to the wall of the sample chamber. The temperature field for a given period depends principally on the end temperatures of the previous periods. After a certain number K of periods, however, the temperature fields of successive periods become identical. When such a steady periodic state is reached, the temperature field is taken as the initial condition for the solution of the energy equation. The number of periods required to attain a steady periodic state depends on the modulation frequency and the thermal diffusivity of the gas. As an example, we obtain $K = 3$ for argon at $T = 304$ K, $p = 0.1015$ MPa, and a modulation frequency of 43 Hz.

From the local temperature rise $\Delta T(t, r, z) = T(t, r, z) - T_w$, the average temperature rise $\Delta\bar{T}(t)$ is

$$\Delta\bar{T}(t) = \frac{1}{V}\int_0^V \Delta T(t, r, z)\, dV \tag{5}$$

where V is the volume of the sample chamber. Temperature and pressure are related through the equation of state $T(p, v)$, with constant specific volume in our case. A Taylor series expansion yields

$$\Delta \bar{T}(t) = \bar{T} - T_0 = \left(\frac{\partial \bar{T}}{\partial p}\right)_{p_0,\, T_0} \Delta p(t) + \cdots \tag{6}$$

$$\Delta \bar{T}(t \to \infty) = \Delta \bar{T}_\infty = \left(\frac{\partial \bar{T}}{\partial p}\right)_{p_0,\, T_0} \Delta p_\infty + \cdots \tag{7}$$

Neglecting terms of higher than first order, due to the small pressure changes, we obtain proportionality between the average temperature rise and the pressure rise

$$\frac{\Delta \bar{T}(t)}{\Delta \bar{T}_\infty} = \frac{\Delta p(t)}{\Delta p_\infty} \tag{8}$$

With Eq. (8) and the expression for $\Delta \bar{T}(t)$ obtained from the analytical solution of the energy equation [7], the pressure rise is

$$\Delta p(t) = \Delta p_\infty \left\{ 1 + \sum_{m=1}^{\infty} K_m \exp\left(-\frac{\zeta_m^2 a t}{R^2}\right) \times \left[1 - \sum_{k=1}^{K} \left\{ \exp\left(-\frac{\zeta_m^2 a (2k-1)}{2R^2 f_{\text{ch}}}\right) - \exp\left(-\frac{\zeta_m^2 a k}{R^2 f_{\text{ch}}}\right) \right\} \right] \right\} \tag{9}$$

At the beginning of a given light phase the time is set to $t = 0$, and K is the number of previous periods. f_{ch} is the modulation frequency of the laser beam, and ζ_m are the zeros of the Bessel function of zero order. K_m are coefficients, dependent on the beam parameters w_0 and C^*, determined by using Eq. (4).

As follows from Eq. (9), the radius of the sample chamber should be kept as small as possible, because with increasing radius, the pressure rise $d\Delta p/dt$ decreases. Consequently, it takes more time for the pressure rise of a light phase to be detected. This time, however, is limited by the lower cutoff frequency of the microphone. A sample chamber with an inner diameter of 1.5 mm and a microphone with a lower cutoff frequency of 0.1 Hz permit measurements down to $a = 1.0 \times 10^{-7}\ \text{m}^2 \cdot \text{s}^{-1}$. The maximum modulation frequency of the laser light of 200 Hz limits the measuring range to thermal diffusivities below $a = 1.0 \times 10^{-3}\ \text{m}^2 \cdot \text{s}^{-1}$.

On the other hand, the microphone of 12.7 mm diameter is mounted next to the tube of 1.5 mm diameter, whereby a clearance volume in front of the microphone cannot be avoided entirely. Moreover, microphones are equipped with a capillary tube that equalizes the static pressure on both sides of the microphone membrane. This capillary tube is designed in such a way that the acoustic pressure is not influenced for sample volumes above 2000 mm^3. In our case the volume of the sample chamber is 170 mm^3. Both the clearance volume and the mass flow in the capillary tube of the microphone induce changes of the density in the sample chamber during the pressure rise so that the assumption of a constant density in the Taylor series expansion, Eqs. (6) and (7), is not longer valid. In order to study the influence of the pressure rise, the mass and the energy balances were solved simultaneously for the system shown in Fig. 3. For an ideal gas, the energy equation for system 1 is

$$\rho c_v \frac{\partial T_1}{\partial t} - \frac{\mathscr{R} T_1}{V_1} \frac{dm_1}{dt} = \lambda \frac{\partial^2 T_1}{\partial r^2} + \frac{\lambda}{r} \frac{\partial T_1}{\partial r} + \mathscr{A}(r) \tag{10}$$

where $\mathscr{R}$ denotes the specific gas constant. The average temperature is

$$\bar{T}_1(t) = \frac{1}{V} \int_0^V T_1(t, r)\, dV \tag{11}$$

The gas velocities w_t in the throttles are obtained from the Bernoulli-equation

$$\frac{1}{2} w_{t1}^2 - \frac{1}{2} w_1^2 + \int_{p_1}^{p_2} \frac{1}{\rho}\, dp + \frac{1}{2} w_{t1}^2 \frac{L_1}{D_1} f = 0 \tag{12}$$

where L_1 is the tube length, D_1 is the diameter, and f the friction factor, which is for laminar flow $f = 64/\mathrm{Re}$. Neglecting the compressibility of the

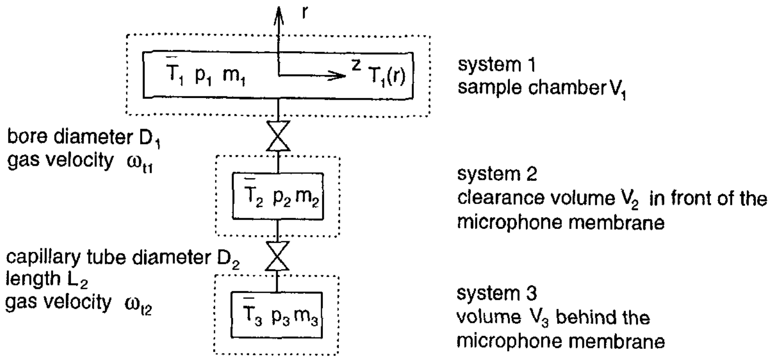

Fig. 3. The model of a nonresonant photoacoustic detector.

gas and the friction in the bore, in Eq. (12), the mass balance of system 1 yields

$$\frac{dm_1}{dt} = -\pi \frac{D_1^2}{4} \rho w_{t1} = -\pi \frac{D_1^2}{4} \sqrt{2\rho(p_1 - p_2)}$$

$$= -\pi \frac{D_1^2}{4} \sqrt{2\rho\mathscr{R}\left(\frac{m_1 \bar{T}_1}{V_1} - \frac{m_2 \bar{T}_2}{V_2}\right)} \tag{13}$$

Under adiabatic conditions the energy and mass balances for systems 2 and 3 are

$$c_v m_2 \frac{d\bar{T}_2}{dt} - (c_v + \mathscr{R})(\bar{T}_2 - \bar{T}_1)\frac{dm_1}{dt} - \mathscr{R}\bar{T}_2 \frac{dm_2}{dt} = 0 \tag{14}$$

$$\frac{dm_2}{dt} = -\frac{dm_1}{dt} - \frac{dm_3}{dt} \tag{15}$$

$$c_v m_3 \frac{d\bar{T}_3}{dt} + (c_v(\bar{T}_3 - \bar{T}_2) - \mathscr{R}\bar{T}_3)\frac{dm_3}{dt} = 0 \tag{16}$$

$$\frac{dm_3}{dt} = \pi \frac{D_2^2}{4} \rho w_{t2} = -8\pi\rho\nu L_2 + \sqrt{64\pi^2\rho^2\nu^2 L_2^2 + \frac{\pi^2 \rho D_2^4 \mathscr{R}}{8}\left(\frac{m_2 \bar{T}_2}{V_2} - \frac{m_3 \bar{T}_3}{V_3}\right)} \tag{17}$$

where ν denotes the kinematic viscosity of the gas. The initial conditions are $T_{1\,(t=0,\,r)} = T_w$, $m_{i\,(t=0)} = p_0 V_i / (\mathscr{R} T_w)$, and $\bar{T}_{i\,(t=0)} = T_w$. The state variables $T_1(r, t)$, $\bar{T}_1(t)$, $\bar{T}_2(t)$, $\bar{T}_3(t)$, $m_1(t)$, $m_2(t)$, and $m_3(t)$ are obtained from numerical solution of Eqs. (10)–(16). The pressure is then obtained with the aid of the equation of state for ideal gases. The microphone signal S is

$$S = k_m k_a (p_2 - p_3) \tag{18}$$

where k_m and k_a are the amplification factors of the microphone and amplifier, respectively. These values are tabulated in the calibration charts of the manufacturer.

The solid curve in Fig. 4 refers to the measured photoacoustic signal for argon at $T = 304$ K and $p = 0.1015$ MPa with 1000 ppm ethane as a trace component. The volumes of the sample chambers were $V_1 = 177\ \text{mm}^3$, $V_2 = 543\ \text{mm}^3$, an $V_3 = 334\ \text{mm}^3$. The absorptivity is $\alpha = 0.17\ \text{m}^{-1}$ and the laser power is $W = 5$ mW. The heat generation according to Eqs. (2) and (3) was determined for an average beam radius of $\bar{\omega} = 0.257$ mm. The

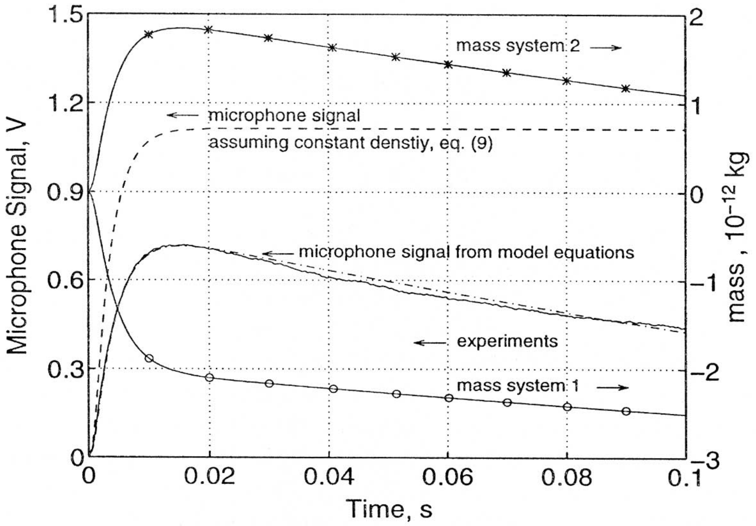

Fig. 4. The photoacoustic signal for argon at $T = 304$ K and $p = 0.1015$ MPa.

dashed-dotted curve is the result of the simulation. It agrees well with the experiments. Between 0 and 0.018 s a high mass flow from system 1 to system 2 and from system 2 to system 3 results in a density decrease in the sample chamber so that the pressure rise is lower than that according to Eq. (9) for constant density, shown by the dashed curve. The pressure decrease after 0.018 s is caused by the mass flow in the capillary tube of the microphone. This mass flow is almost constant.

As the results clearly indicate, the clearance volume in front of the microphone membrane has to be kept as small as possible. It should be lower than 5% of the volume of the sample chamber. Additional flow resistances between both sides of the membrane are useful to reduce the mass flow inside the microphone.

3. THE RESONANT PHOTOACOUSTIC DETECTOR

Figure 2 shows the setup of a resonant photoacoustic detector. The sample chamber, the microphone chamber, and the coupling tube form an acoustic resonator, a so-called Helmholtz resonator. The gas in the coupling tube behaves as if it were moved as a plunger toward one chamber and thus compresses the gas there, whereas the gas in the other chamber expands. The resulting pressure difference between the chambers provides a restoring force accelerating the plunger in the reverse direction.

The oscillation thus generated is damped due to the friction of the wall. The damping factor δ and the angular frequency ω of the oscillations are [7]

$$\delta = -\frac{4\pi\eta}{A\rho} \quad \text{and} \quad \omega = \sqrt{\frac{Av_s^2}{L_R V_2} - \frac{16\pi^2\eta^2}{A^2\rho^2}} \tag{19}$$

where v_s is the velocity of sound, η the viscosity, A the cross-sectionional area, and L_R the length of the coupling tube.

By means of a resonant detector, reference measurements with argon lead to an uncertainity of less than ±1%, although the clearance volume in front of the microphone is greater than that of the nonresonant cell. As in the case of harmonic oscillations, the mass flows are oscillating too, but the time-averaged density in the chamber remains constant. The pressure rise can be understood as a superposition of the pressure rise according to Eq. (9) and damped harmonic oscillations. Therefore, the dashed curve in Fig. 5, referring to the pressure rise according to Eq. (9), intersects the measured curve at its inflection points.

A serious disadvantage of the resonant detector is that accurate results are obtained only when the harmonic oscillations are not too intensively damped, otherwise the density change in the sample chamber is too great.

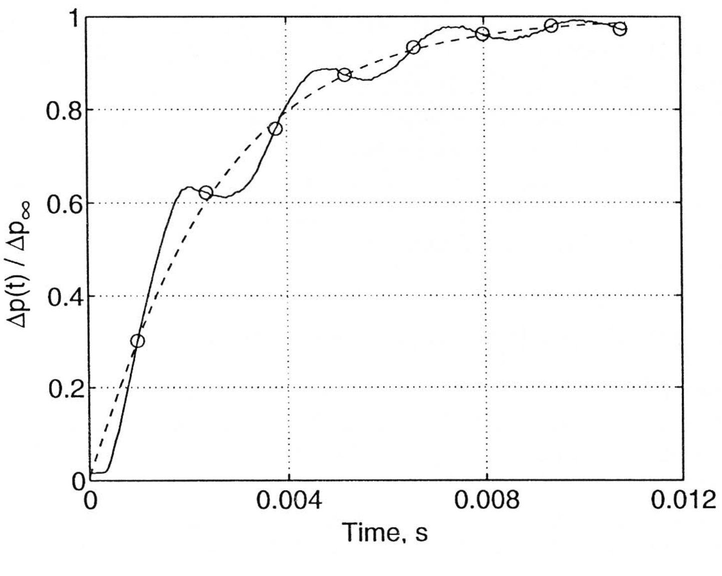

Fig. 5. Helmholtz oscillations in a resonant photoacoustic detector.

4. SUITABLE TRACE GASES

Previous experiments were made with argon as a test gas [7, 8] with a helium–neon laser at a wavelength of 3.39 μm, corresponding to a wave number of 2950 cm^{-1}. Around this wavelength the infrared spectra of hydrocarbons and refrigerants have strong absorption bands caused by transitions to a higher vibrational level of the C–H bond. A trace gas therefore is not needed. The pressure range, however, is limited to pressures below 0.01 MPa. Otherwise, the absorbed radiation energy is too high. If the absorbed energy is more than 5% of the incoming energy, axial temperature gradients cannot be neglected and thus Eq. (9) is no longer valid. Hydrocarbons, in general, do not absorb at a wavelength of 1.531 μm, where ammonia has a local absorption maximum with a line strength of $S = 1.85 \times 10^{-21}$ cm/molecule at $T = 293$ K. Assuming a Lorentz profile and a line width of $\nu = 0.1\ \text{cm}^{-1}$, it is recommended to add ammonia with a partial pressure of at least 300 Pa in order to achieve a sufficiently high absorptivity coefficient of about 0.09 m^{-1}. This value leads to an adequate photoacoustic signal, so that measurements can be carried out at pressures above 0.1 MPa without affecting the thermophysical properties of the test gas. In the pressure range between 0.01 and 0.1 MPa, the ammonia added to the test gas changes the thermal diffusivity, the density and the isochoric heat capacity. The errors thus introduced must be corrected.

5. CONCLUSION

A nonresonant photoacoustic detector is an efficient measurement device for precise measurements of thermal diffusivities in the range between 1.0×10^{-3} and $1.0 \times 10^{-7}\ \text{m}^2 \cdot \text{s}^{-1}$. Such a nonresonant cell should be preferred because measurements can be performed for a range of thermal diffusivities that is almost a factor of 100 wider than the range that can be obtained with a resonant cell.

Measurements with refrigerants at pressures below 0.01 MPa can be carried out with a helium–neon laser at an emission wavelength of 3.39 μm. As the refrigerants show strong absorption bands around this wavelength, a trace gas is not needed. In this pressure range the refrigerants can be considered as ideal gases, so that the measured thermal diffusivities can be easily converted into thermal conductivities. Above 0.1 MPa the thermal diffusivity of refrigerants can be measured by adding ammonia as a trace gas.

As the model clearly indicates, the clearance volume in front of the microphone should be kept below 5% of the volume of the sample chamber. Due to the small volume of the sample chamber, the mass flow in the capillary tube connecting both sides of the membrane should be minimized.

REFERENCES

1. V. Vesovic, W. A. Wakeham, G. A. Olchowy, J. V. Sengers, J. T. R. Watson, and J. Millat, *J. Phys. Chem. Ref. Data* **19**:763 (1990).
2. A. Laesecke, R. Krauss, K. Stephan, and W. Wagner, *J. Phys. Chem. Ref. Data* **19**:1089 (1990).
3. W. A. Wakeham, A. Nagashima, and J. V. Sengers, in *Experimental Thermodynamics, Vol. III* (Blackwell Scientific, Oxford, 1991), Chap. 7.
4. B. Taxis and K. Stephan, *Int. J. Thermophys.* **15**:141 (1994).
5. Y. Tanaka, M. Nakata, and T. Makita, *Int. J. Thermophys.* **12**:949 (1991).
6. B. Kruppa and J. Straub, *Fluid Phase Equil.* **80**:305 (1992).
7. J. Soldner and K. Stephan, *Proceedings of the 2nd European Thermal-Sciences and 14th UIT National Heat Transfer Conference, Rome* **2**:1071 (1996).
8. J. Soldner and K. Stephan, *Proceedings of the 23rd International Thermal Conductivity Conference, Nashville* **1**:481 (1996).